Separation of Polystyrene Microbeads Using Dielectrophoretic/ Gravitational Field-Flow-Fractionation

Xiao-Bo Wang, Jody Vykoukal, Frederick F. Becker, and Peter R. C. Gascoyne
Department of Experimental Pathology, University of Texas M. D. Anderson Cancer Center, Houston, Texas 77030 USA

ABSTRACT The characterization of a dielectrophoretic/gravitational field-flow-fractionation (DEP/G-FFF) system using model polystyrene (PS) microbeads is presented. Separations of PS beads of different surface functionalization (COOH and none) and different sizes (6, 10, and 15 μm in diameter) are demonstrated. To investigate the factors influencing separation performance, particle elution times were determined as a function of particle suspension conductivity, fluid flow rate, and applied field frequency and voltage. Experimental data were analyzed using a previously reported theoretical model and good agreement between theory and experiment was found. It was shown that separation of PS beads was based on the differences in their effective dielectric properties. Particles possessing different dielectric properties were positioned at different heights in a fluid-flow profile in a thin chamber by the balance of DEP and gravitational forces, transported at different velocities under the influence of the fluid flow, and thereby separated. To explore hydrodynamic (HD) lift effects, velocities of PS beads were determined as a function of fluid flow rate in the separation chamber when no DEP field was applied. In this case, particle equilibrium height positions were governed solely by the balance of HD lift and gravitational forces. It was concluded that under the experimental conditions reported here, the DEP force was the dominant factor in controlling particle equilibrium height and that HD lift force played little role in DEP/G-FFF operation. Finally, the influence of various experimental parameters on separation performance was discussed for the optimization of DEP/G-FFF.

INTRODUCTION

Dielectrophoresis (DEP) is the translational movement of a particle in a nonuniform AC electric field driven by a force arising from the electrostatic interaction between field-induced polarization in the particle and the applied nonuniform field (Fuhr et al., 1996; Jones, 1995; Pethig, 1991; Pohl, 1978; Wang et al., 1995b). DEP fields are generated by electrode structures of appropriately designed geometry such as the pin-plate, isomotive, polynomial, or castellated interdigitated forms (Huang and Pethig, 1991; Marszalek et al., 1989; Pohl and Pollock 1978; Pethig et al., 1992). Early studies of dielectrophoresis used electrode structures made from thin metal wires, needles, or plates (Pohl and Pethig, 1977; Jones and Kraybill, 1986), while modern dielectrophoresis employs microfabrication technology to produce microelectrode arrays capable of producing sufficiently large DEP forces to induce particle motion with small applied voltages (e.g., Burt et al., 1990; Fuhr et al., 1992; Gascoyne et al., 1992; Wang et al., 1995a). DEP forces are dependent on the spatial distributions of applied electrical fields as well as the dielectric properties of particles and of their surrounding medium. Because of these dependencies, DEP has been exploited for particle characterization (e.g., Gascoyne et al., 1994), manipulation (e.g., Fuhr et al., 1992; Wang et al., 1997), and separation (e.g., Gascoyne et al., 1992, 1997; Talary et al., 1995).

There are several approaches by which DEP can be applied for the separation of particles. In *DEP migration*, particles possessing different dielectric properties are subjected to DEP forces and are caused to migrate differentially to strong or weak electrical field regions. Spatial separation of particles is achieved when particles are focused at different locations on the electrode structure (Gascoyne et al., 1992; Wang et al., 1993). Several techniques of continuous particle separation using this principle have been envisaged (H. A. Pohl, Continuous dielectrophoretic cell classification method, U.S. Patent 4,326,934, 1982; S. Crane, Dielectrophoretic cell stream sorter, U.S. Patent 5,489,506, 1996). According to one scheme, particles are continuously introduced into a separation chamber at a single inlet point and are carried through the chamber by fluid flow. DEP forces are imposed by electrode structures on the chamber walls and these forces induce continuous particle deflection in the plane normal to the direction of the fluid flow and parallel to the chamber bottom. Particles possessing different properties emerge at the outlet of the chamber at different positions depending on the direction and magnitude of the DEP forces experienced. Other methods of DEP separation utilize a combination of DEP and other forces. In *DEP retention*, DEP forces are applied to compete with fluid-flow forces. Particles experiencing large positive DEP forces are trapped at their minimum DEP potential energy positions. Other particles experiencing small positive or negative DEP forces are carried away with the fluid (Markx et al., 1994; Wang et al., 1993). Cell separations of clinical importance using DEP retention have been demonstrated by

Received for publication 5 November 1997 and in final form 5 February 1998.

Address reprint requests to Xiao-Bo Wang, Department of Experimental Pathology, Box 89, University of Texas M. D. Anderson Cancer Center, 1515 Holcombe Boulevard, Houston, TX 77030. Tel.:713-792-7605; Fax: 713-792-5940; E-mail: xiaobo@solace.mdacc.tmc.edu.

0006-3495/98/05/2689/13 $2.00

Becker et al. (1995), Gascoyne et al. (1997), and Talary et al. (1995).

Recently, DEP forces have been combined with field-flow-fractionation (FFF, Giddings, 1989, 1993) for particle separation (Gascoyne et al., 1996; Huang et al., 1997; Markx et al., 1997). The idea of using DEP forces in a FFF system was first suggested by Davis and Giddings (1986) in their theoretical study of dielectric FFF. It was proposed that DEP forces generated by electrodes on the facing walls of an annular channel could be used in conjunction with fluid-intrinsic diffusion forces to generate particle equilibrium concentration profiles across the radial direction of the channel. In this scheme, particles (<1 μm in diameter) having different dielectric or diffusive properties would exhibit different characteristic concentration profiles and would move at different velocities under the influence of fluid-flow. Therefore, they would exit the channel at different times when a flow velocity profile was set up inside. This approach (Davis and Giddings, 1986) of combining DEP with normal FFF was later discussed by Washizu et al. (1994) for a different electrode structure. The DEP-FFF technique reported recently (Gascoyne et al., 1996; Huang et al., 1997; Markx et al., 1997) exploits the balance between dielectrophoretic and gravitational (sedimentational) forces. In this method negative DEP forces are produced by microelectrodes on a chamber and levitate particles to equilibrium positions in a flow-velocity profile. Particles at different heights in the flow stream move at different velocities and can be fractionated based upon their different retention times in the chamber. This technique can be termed dielectrophoretic/gravitational-FFF (DEP/G-FFF), a subtechnique of DEP-hyperlayer-FFF. Balancing DEP forces with other types of physical forces (e.g., electrophoretic, cross-flow, or DEP forces generated from different electrodes in the chamber) results in other subtechniques such as DEP/electrophoretic-FFF.

Field-flow-fractionation has been used for separation and characterization of a number of types of biological cells including *Escherichia coli*, human and animal erythrocytes, cultured human HeLa, and Chinese hamster ovary CHO-K1 cells (Andreux et al., 1993; Berg and Turner, 1991; Caldwell et al., 1984; Cardot et al., 1992; Parsons et al., 1996; Tong et al., 1997). FFF studies of human erythrocytes have revealed that cell membrane deformability is an important factor contributing to the hydrodynamic lifting force acting on the cells as they travel in the flow stream at positions close to the channel walls (Tong and Caldwell, 1995). In recent DEP/G-FFF studies, cell equilibrium heights and velocities were shown to be dependent on cell dielectric properties and on the frequency and voltage of applied signals (Gascoyne et al., 1996; Huang et al., 1997; Markx et al., 1997). Separation of normal human mononuclear cells and human leukemia (HL-60) cells based on differential DEP/G-FFF velocities was demonstrated and a theoretical model was developed to account for the experimental data (Huang et al., 1997).

Here we report the construction and characterization of a complete DEP/G-FFF system consisting of a syringe pump, a fluid-sample-injector, a DEP/G-FFF chamber, and a particle detector at the chamber outlet. The separations of model particles of polystyrene (PS) microbeads having different surface functionalizations (COOH and none) and different sizes (6, 10, and 15 μm in diameter) are demonstrated. Separation performance is shown to be a function of the suspension conductivity, the fluid flow rate, and the voltage and frequency of the signals applied to the electrode. A theoretical analysis of the results reveals that separation of PS microbeads is based upon the differences in the effective dielectric properties of different bead types.

MATERIALS AND METHODS

DEP/G-FFF system

A schematic representation of the DEP/G-FFF system is shown in Fig. 1. Parallel microelectrode arrays having 50-μm widths and gaps were fabricated on 50 $\times$ 50-mm glass substrates using standard photolithographic methods. Eight 50 $\times$ 50 mm electrode plates were glued end-to-end onto a supporting glass plate to form an electrode of area 50 $\times$ 400 mm. A Teflon spacer (H 0.4 $\times$ W 50 $\times$ L 400 mm) was cut to provide an open channel with dimensions of 388 mm from tip to tip and 25 mm in width except at the tapered ends. This was sandwiched between the bottom electrode plate and a top glass plate to form the DEP/G-FFF chamber. The chamber was firmly assembled with 36 Nylon screw-clamps (Bel-Art Products, NJ). The top and bottom plates were drilled with 0.0625-in. diameter holes to fit inlet and outlet tubing at positions coincident with the points of the tapered opposite ends of the cutout channel. Microelectrode arrays, each having two 4-mm wide electrical conductor buses running along the edges, were connected in parallel to a lab-built PA05-based power amplifier (Apex Microtechnology, AZ). The amplifier could deliver up to 10 W of power into a 2-ohm load with a bandwidth of DC to 400 kHz.

A digital syringe pump (KD Scientific, MA) was used to provide continuous flow of carrier medium through the DEP/G-FFF chamber at a rate selectable between 1 μl/min and 70 ml/min. A sample injection valve (Rheodyne Model 7010, CA) allowed measured sample introduction from a 10-μl loop. A 5-cm length of PEEK tubing (0.0625 in. OD, 0.010 in. ID) having a void volume of 2.5 μl served as the inlet connection between the injection valve and the chamber.

Two different methods were used to characterize particle responses in the DEP/G-FFF chamber. The first approach was to manually gauge the dynamics of particle separation by counting particles that passed by several specific inspection locations along the length of the chamber as a function of time with the aid of video microscopy. The second method was to monitor particles exiting the chamber with a UV detector. To accomplish this, the chamber outlet was connected to the 3-μl flow cell of a UV spectroscopic detection system (ISCO Model UA-6, NE) via a 5-cm length of PEEK tubing (0.0625 in. OD, 0.020 in. ID). The detector was operated at a wavelength of 254 nm and its output voltage signal, proportional to light attenuation by particles in the flow-cell, was fed to a chart recorder (Goetz, Austria).

PS bead preparation

Two types of experiments were conducted: 1) separation of PS beads (Polysciences, PA) of similar density (1050 kg/m^3) and size (9.44 $\pm$ 0.95 vs. 10.57 $\pm$ 1.03 μm in diameter), but possessing different surface functionalizations (COOH and none); and 2) separation of nonfunctionalized PS (NF-PS) beads of similar density (1050 kg/m^3) but of different sizes (6.14 $\pm$ 0.45, 10.57 $\pm$ 1.03, and 15.5 $\pm$ 1.84 μm). Surface-carboxylated (COOH-PS) beads were characterized by the manufacturer as having a

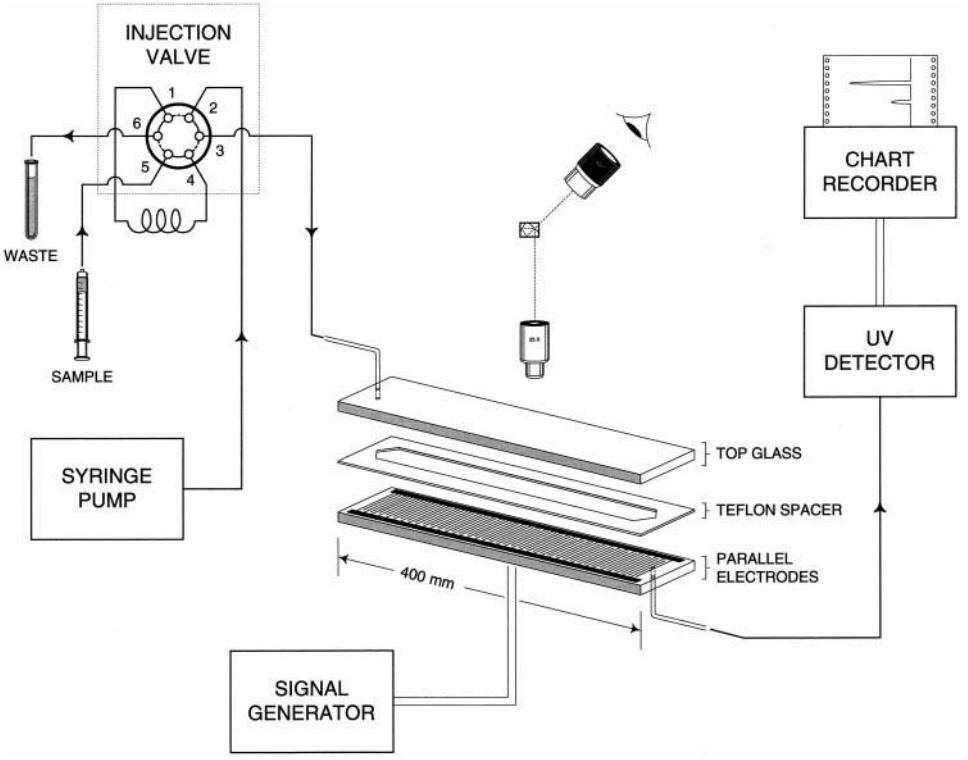

FIGURE 1 Schematic representation of the DEP/G-FFF system showing the chamber in exploded view to reveal the Teflon spacer with the flow channel cut into it. The operation of the injection valve is as follows: the sample is first loaded into the loop through the path "syringe→5→4→loop→1→6→waste" with fluid flow in the second path; in the injection mode, the fluid flow path is "syringe pump→2→1→loop→4→3→chamber."

surface charge of 0.12 mEq (COO^-)/g of polymer. While there are other methods suitable for the separation of PS beads, these beads were chosen as model particles in this study to aid in the characterization and development of the DEP/G-FFF system because they were relatively homogeneous in terms of size, density, and other structural and compositional characteristics.

Our standard DEP buffer, consisting of 8.5% (w/v) sucrose and 0.3% (w/v) dextrose, was used as the FFF carrier fluid and particle-suspending medium. Electrical conductivity of the buffer was brought to 2.2 or 10 mS/m with aliquots of 300 mM EDTA (adjusted to pH 7.0 with NaOH). The final pH of the buffer was found to be ~6.8. To ensure that no air bubbles were present in the DEP/G-FFF chamber during separation, the sucrose/dextrose buffer was degassed under vacuum for several minutes. Sample mixtures were prepared by diluting aliquots of Polysciences-supplied microbead suspensions with the sucrose/dextrose buffer to achieve particle concentrations of 1.5×10^7, 3×10^6, and 4×10^5 particles/ml for PS beads of nominal diameter 6, 10, and 15 μm, respectively.

Bead separation protocol

The DEP/G-FFF chamber was first loaded with carrier medium (sucrose/dextrose buffer) using the syringe pump; precautions were taken to ensure that no air bubbles were introduced into the chamber. Appropriate voltage signals (between 0.5 and 1 V RMS at 50 kHz) were then applied to the microelectrodes so that PS beads would be levitated to equilibrium positions upon injection into the chamber, thereby minimizing contact and possible adherence of the beads to the electrode surface. Next, a mixture of PS bead types was introduced into the chamber. To accomplish this, the injection valve was first set in the "load" mode and the 10-μl loop was filled with sample using a manually operated syringe. The valve was then switched to the "injection" mode and 35 μl sucrose/dextrose buffer was pumped through the loop by the syringe pump operating at 50 μl/min to flush the beads into the DEP/G-FFF chamber. The valve was then switched back to the "load" mode, ready for the next sample loading.

After PS microbeads had been loaded into the inlet port of the chamber, they were allowed to relax for some minutes (up to 30 min) in order to attain equilibrium height positions where the sedimentation and DEP levitation forces were balanced. Following relaxation, flow of the carrier medium was initiated in the chamber from the syringe pump, which was operated at a desired flow rate in the range 20–2000 μl/min. As PS beads were carried along the chamber length, their kinetics were observed with video microscopy (Nikon Microphot-SA microscope, Hamamatsu XC-77 CCD camera) and results were recorded on a VCR (Panasonic, AG-7350). Finally, PS beads exiting the chamber were monitored by the UV detection system.

RESULTS

Separation dynamics

To examine the dynamic process of DEP/G-FFF separation, we followed particle trajectories in the chamber by monitoring the number of particles that passed by several inspection windows along the chamber as a function of time. From these data we constructed three-dimensional representations of separation dynamics where the number (z axis) of particles was plotted as a function of time (x axis) at different inspection positions (y axis) along the chamber. A typical example is shown in Fig. 2 for a DEP/G-FFF separation of NF-PS and COOH-PS beads. Clearly, the two subpopulations of beads traveled at different velocities and became more and more separated as they moved further along the chamber. A single peak was only visible at position 1. Thereafter, bifurcation of the peak occurred until two distinct (nonoverlapping) peaks were observed at position 5 (165 mm from the chamber inlet). This indicates that complete separation of the two bead subpopulations could be achieved with a chamber only 165 mm long. By the time the

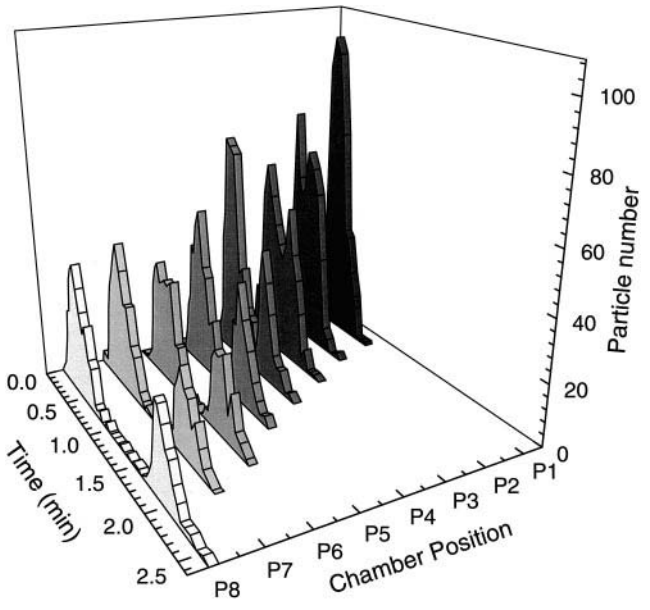

FIGURE 2 Three-dimensional representation of DEP/G-FFF fractionation of NF-PS (10.57 ± 1.03 μm) and COOH-PS (9.44 ± 0.95 μm) beads. Particle counts were plotted as a function of time at eight inspection locations having distances of 36, 64, 92, 132, 165, 225, 272, and 360 mm from the chamber inlet. To show the progress of separation, the time *after the emergence of the first bead at each position* was used to define *zero time* for that location. A single peak was detected only at position 1 (36 mm from the chamber inlet). Two overlapping peaks appeared at position 2 and these become more and more widely separated at positions 3–8. Conditions: voltage, 1.6 V RMS at 50 kHz; parallel electrode arrays, 50 μm electrode widths and gaps. After injection, beads were allowed to relax to their equilibrium height positions in the chamber for 10 min prior to the application of the fluid flow. To begin separation, flow of sucrose buffer of electrical conductivity 10 mS/m was initiated at 200 μl/min.

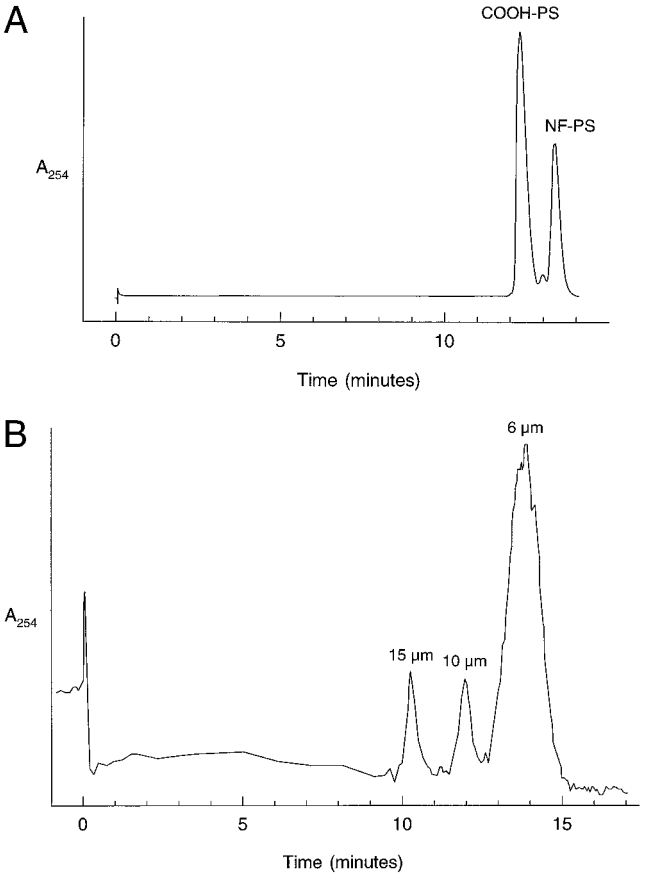

FIGURE 3 (*A*) DEP/G-FFF fractogram showing the separation of NF-PS (10.57 ± 1.03 μm) and COOH-PS (9.44 ± 0.95 μm) beads. Conditions: voltage, 1.24 V RMS at 50 kHz; parallel electrode arrays, 50 μm electrode widths and gaps. Beads were allowed to relax to their equilibrium height positions in the chamber for 10 min after injection and before the application of fluid flow. Sucrose buffer of electrical conductivity 10 mS/m was pumped through the chamber at 800 μl/min. (*B*) DEP/G-FFF fractogram showing the separation of NF-PS beads of different sizes (6.14 ± 0.45, 10.57 ± 1.03, and 15.5 ± 1.84 μm in diameter). Conditions: voltage, 0.53 V RMS at 100 kHz; parallel electrode arrays, 50 μm electrode widths and gaps. Beads were allowed to relax for 25 min after injection and before the application of fluid flow. Sucrose buffer of electrical conductivity 2.2 mS/m was pumped through the chamber at 800 μl/min.

beads reached position 8 (close to the chamber outlet and 360 mm from the inlet), the two subpopulation peaks were separated by a time interval of >1 min.

DEP/G-FFF fractograms

To characterize the separation performance, particles exiting the DEP/G-FFF chamber were monitored using the UV detector. Typical fractograms displaying the time dependence of the UV absorbance are shown in Fig. 3, *A* and *B*. Fig. 3 *A* depicts the separation of COOH-PS and NF-PS beads with the two peaks occurring 11.7–12.4 and 12.8–13.4 min after the initiation of fluid flow, respectively. In order to associate elution times with specific microbead types, DEP/G-FFF experiments were performed on pure NF-PS or COOH-PS beads and then on several mixtures of these bead types at different concentration ratios. By comparing the elution peak times in these experiments, we determined that the COOH-PS beads eluted ahead of the NF-PS beads. Fig. 3 *B* shows the separation of NF-PS beads of three different sizes (nominal diameters 6, 10, and 15 μm). Direct observation of particle motion under the microscope revealed that larger beads moved faster than smaller ones. Thus, the three elution peaks in time range of 9.9–10.8, 11.6–12.4, and 12.7–15 min corresponded to populations of 15, 10, and 6 μm diameters, respectively.

Separation of NF-PS and COOH-PS beads

We (Huang et al., 1997) and others (Tong and Caldwell, 1995; Williams et al., 1992) have previously reported that particles experience a hydrodynamic (HD) lifting force that pushes them away from the chamber walls as they are carried along in a fluid flow profile. This lifting force was shown to increase with the fluid flow rate (Williams et al., 1992). To determine the influence of the HD lifting force on overall particle kinetics, separation experiments were conducted as a function of the fluid flow rate for a specified DEP field condition. As shown in Fig. 4, *A* and *B*, the

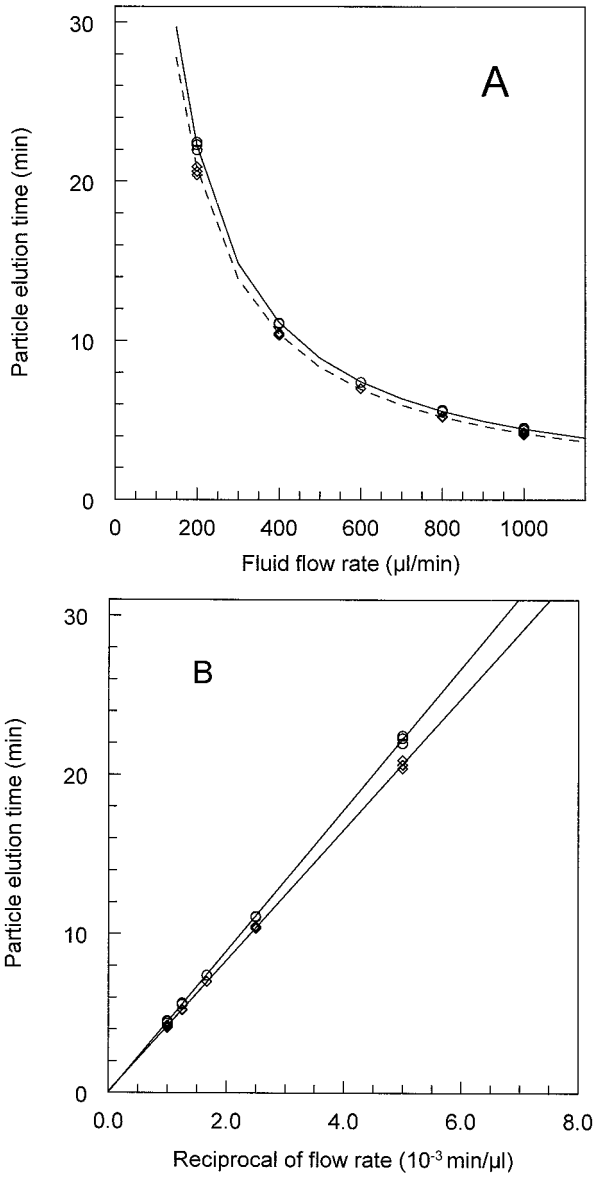

FIGURE 4 (*A*) Dependency of elution peak times for NF-PS (10.57 ± 1.03 μm, ○) and COOH-PS (9.44 ± 0.95 μm, ◇) beads on the fluid flow rate in DEP/G-FFF separation. Particle suspension conditions are the same for Fig. 3 *A*. Conditions: voltage, 1.6 V RMS at 50 kHz; parallel electrode arrays, 50 μm electrode widths and gaps. The continuous lines represent the theoretical-fit of experimental data using Eqs. 2–7. Values for the dielectric parameter Re(f_{CM}) at 50 kHz were derived as −0.20 and −0.28 for NF-PS and COOH-PS beads suspended in aqueous medium of conductivity 10 mS/m, respectively. (*B*) Plot of elution peak times for NF-PS and COOH-PS beads versus the reciprocal of the fluid flow rate. The solid line is a linear fit to the experimental data.

elution peak times for NF-PS and COOH-PS beads were inversely proportional to the flow rate in the range of 100 to 1000 μl/min. Separation effectiveness, as characterized by the ratio of the elution peak times for two PS bead populations, was not compromised even at the high flow rate of 1000 μl/min. As discussed later, these results indicate that the hydrodynamic lifting force played little role in the separation process for the flow rate range investigated here.

The importance of DEP forces in DEP/G-FFF separation is illustrated in Fig. 5 *A*, where elution peak times for NF-PS and COOH-PS beads are shown as a function of the applied DEP voltage signals. Increasing the applied voltage from 0.07 V to 2.65 V RMS resulted in faster elution of both

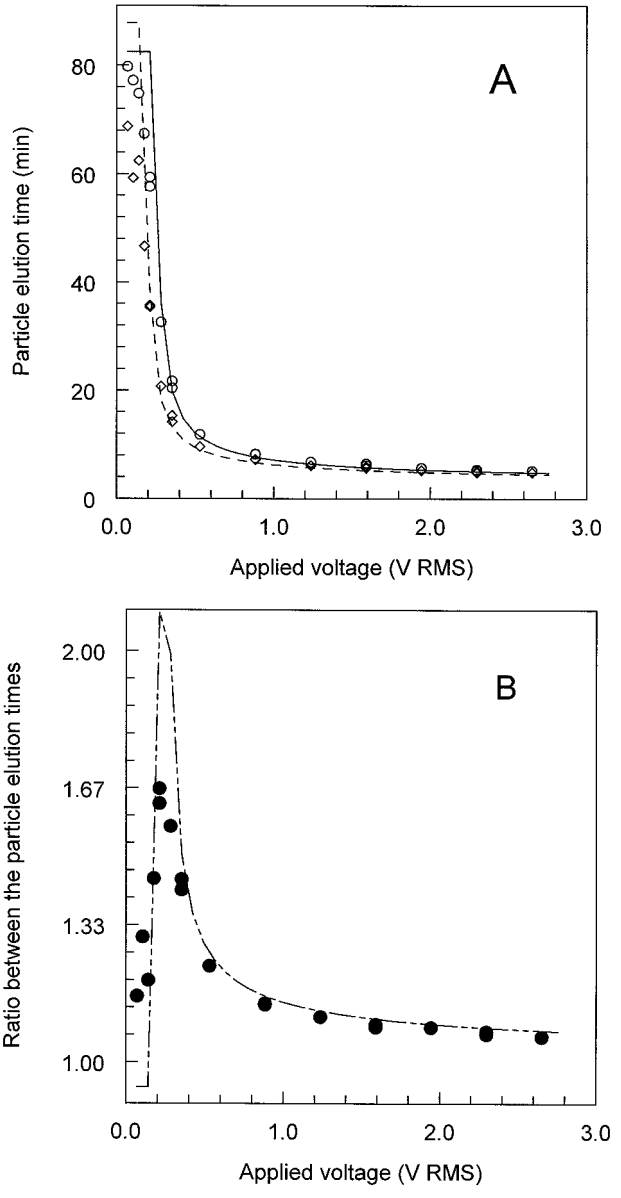

FIGURE 5 (*A*) Dependency of elution peak times for NF-PS (10.57 ± 1.03 μm, ○) and COOH-PS (9.44 ± 0.95 μm, ◇) beads on the voltage (50 kHz) applied to the microelectrodes. (*B*) Plot of the ratio of the two elution peak times for NF-PS and COOH-PS beads versus the applied voltage. Particles were allowed to relax in the chamber for 10 min after injection and before the application of fluid flow. Sucrose buffer of electrical conductivity 10 mS/m was pumped through the chamber at a rate of 800 μl/min. The continuous lines represent the best fits of Eqs. 2–7 to the experimental data. Values for dielectric parameter Re(f_{CM}) at 50 kHz were thereby derived as −0.18 and −0.30 for NF-PS and COOH-PS beads suspended in aqueous medium of conductivity 10 mS/m, respectively. At the applied voltage of 0.53 V (RMS), particle equilibrium heights are calculated from their retention times using Eqs. 2, 3, and 7 to be 29.1 and 41.2 μm for NF-PS and COOH-PS beads, respectively.

NF-PS and COOH-PS beads. This is expected when it is considered that larger applied voltages levitate particles to higher equilibrium position in the flow velocity profile (Gascoyne et al., 1996; Huang et al., 1997). Separation effectiveness was observed to be a function of the applied voltage (Fig. 5 *B*). The best separation of the two bead populations, as characterized by a maximum value of ~1.65 for the ratio of the two elution peak times, was attained at an applied voltage of 0.21 V RMS. Increasing or decreasing the applied voltage resulted in a gradual convergence of the two elution peaks.

Separation of NF-PS beads of three different sizes

The dependence of elution times on the applied DEP voltage is shown in Fig. 6 for PS beads of nominal diameter 6, 10, and 15 μm. As for the separation of NF-PS and COOH-PS beads, an increase in the applied voltage resulted in decreased bead elution times and decreased separation between the three elution peaks. Separation of NF-PS beads of 6, 10, and 15 μm was also studied as a function of the applied field frequency for constant fluid flow and applied voltage conditions (Fig. 7). The elution-peak time for 15-μm beads remained nearly constant in the frequency range 1 to 400 kHz. For 10-μm beads, the elution time was nearly constant in the frequency range 5 to 200 kHz but became larger at lower (1–2 kHz) or higher (400 kHz) frequencies. Strong frequency dependency with a maximum elution time at 50 kHz was exhibited by 6-μm beads. Optimum separation of these beads was achieved at ~50 kHz.

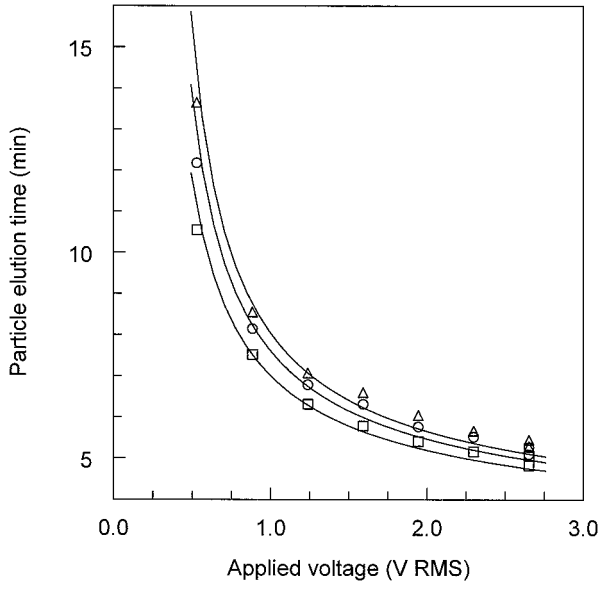

FIGURE 6 Dependency of elution peak times for NF-PS beads of 6 (△), 10 (○), and 15 (□) μm diameter on the voltage (50 kHz) applied to the microelectrode array. Particles were allowed to relax to equilibrium height positions in the chamber for 25 min after injection and before the application of fluid flow. Sucrose buffer of electrical conductivity 2.2 mS/m was pumped through the chamber at a rate of 800 μl/min. The solid lines represent the best fit of theory to the experimental data according to Eqs. 3–8. Values for the dielectric parameter Re(f_{CM}) at 50 kHz were derived as −0.12, −0.14, and −0.19 for 6, 10, and 15-μm beads, respectively, suspended in aqueous medium of conductivity 2.2 mS/m. Particle equilibrium heights are calculated from their retention times using Eqs. 2, 3, and 7 to be 22.1, 25, and 30 μm for 6, 10, and 15 μm beads, respectively, at the smallest applied voltage of 0.53 V (RMS).

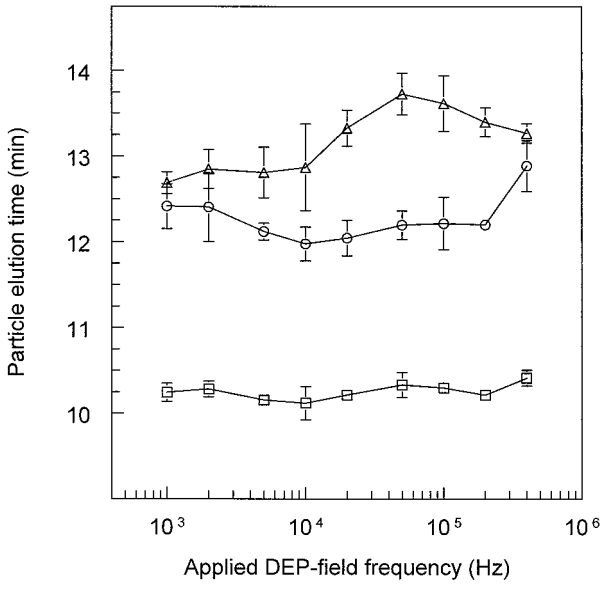

FIGURE 7 Dependency of elution peak times for PS beads of 6 (△), 10 (○), and 15 (□) μm diameter on the applied field frequency. The voltage of the applied electrical signals was 0.53 V RMS. Particles were allowed to relax to their equilibrium height positions in the chamber for 25 min prior to the application of fluid flow. Sucrose buffer of electrical conductivity 2.2 mS/m was pumped through the chamber at a rate of 800 μl/min.

DISCUSSION

Bead relaxation

A common requirement of most FFF methods (Liu et al., 1991; Caldwell and Gao, 1993) is allowing particles to be separated to relax to equilibrium positions with respect to the surfaces of the separation chamber before the fluid-flow is started. Equilibrium positions are reached when the physical forces that act on the particles are balanced. The relaxation process ensures that the differential positions of the particles in the fluid-flow profile, and the corresponding particle velocities and transit times across the chamber, depend only on the physical properties of the particles and not on their initial positions after introduction into the chamber. Therefore, after they were introduced into the DEP/G-FFF chamber, PS beads were allowed to sediment to their equilibrium heights with appropriate DEP electrical fields applied. The time (t_r) required for a particle of radius r and density ρ_p to sediment a distance H can be readily derived from the formula

$$t_r = \frac{9H\eta}{2(\rho_p - \rho_m)r^2 g} \quad (1)$$

where g is the acceleration due to gravity and ρ_m and η are the density and viscosity of the suspending medium, respectively. Equation 1 reveals that small particles will take longer to relax than larger particles. For example, the relaxation times for PS beads of 6, 10, and 15 μm diameter (density 1050 kg/m^3) are ~4, 9, and 25 min, respectively, for a relaxation distance of 400 μm in a medium of density 1033 kg/m^3 and viscosity 1.26×10^{-3} kg · m · s.

DEP/G-FFF chamber surface treatment

As discussed above, PS beads should theoretically settle to their equilibrium height positions as determined by the balance of sedimentation and applied DEP forces during relaxation. However, the DEP levitation force is larger above the electrode edges of the electrode array and smaller over the centers of the electrodes and gaps (Fig. 8 *A*). As a result of this as well as certain imperfections such as occasional open circuits in electrode elements, some PS beads may settle to the chamber bottom surface. These may adhere to the chamber wall, where they can disturb the laminar flow profile when fluid flow is started, and impair the separation performance. Therefore, after several experiments we realized that an appropriate conditioning of the chamber bottom surface to inhibit particle adherence was critical to achieving optimum separation results. The following procedures were developed for chamber surface treatment. Electrodes were first washed in 1% (w/v) Alconox detergent (Alconox Inc., NY), rinsed thoroughly with deionized water, and air-dried before chamber assembly. To remove any residual water in the chamber, it was filled with ethanol and then dried with filtered, low-pressure N_2. The chamber was then filled with Sigmacote (Sigma, MO) for 15 min and dried again with N_2. Each Sigmacote treatment, which applied a hydrophobic coating to the chamber walls, lasted for ~20 experiments. After each day's usage the chamber was flushed with 60 ml of 1% (w/v) Alconox plus 0.05% (w/v) NaOCl (Clorox Inc., CA) solution at 2 ml/min for 30 min. For overnight storage the chamber was filled with this solution to ensure there was no growth of microorganisms. The chamber can be used for many hundreds of experiments without noticeable changes in its separation performance, provided the electrode surface treatment described above is performed regularly.

Particle kinetics

As illustrated in Fig. 9, a particle traveling in a DEP/G-FFF chamber experiences several forces. In the vertical direction, DEP levitation, sedimentation (gravitation), and HD lift forces act to determine the particle height in the fluid-flow profile. Because of the nonuniform nature of the electric field distribution in the chamber, the DEP levitation force varies with particle position relative to the electrode structure, as depicted in the vector representation of DEP force distribution reported earlier (Huang et al., 1997; Wang et al., 1996). Larger DEP forces are experienced by a particle when it is directly above the electrode edges than when it is above the central regions of electrodes and gaps

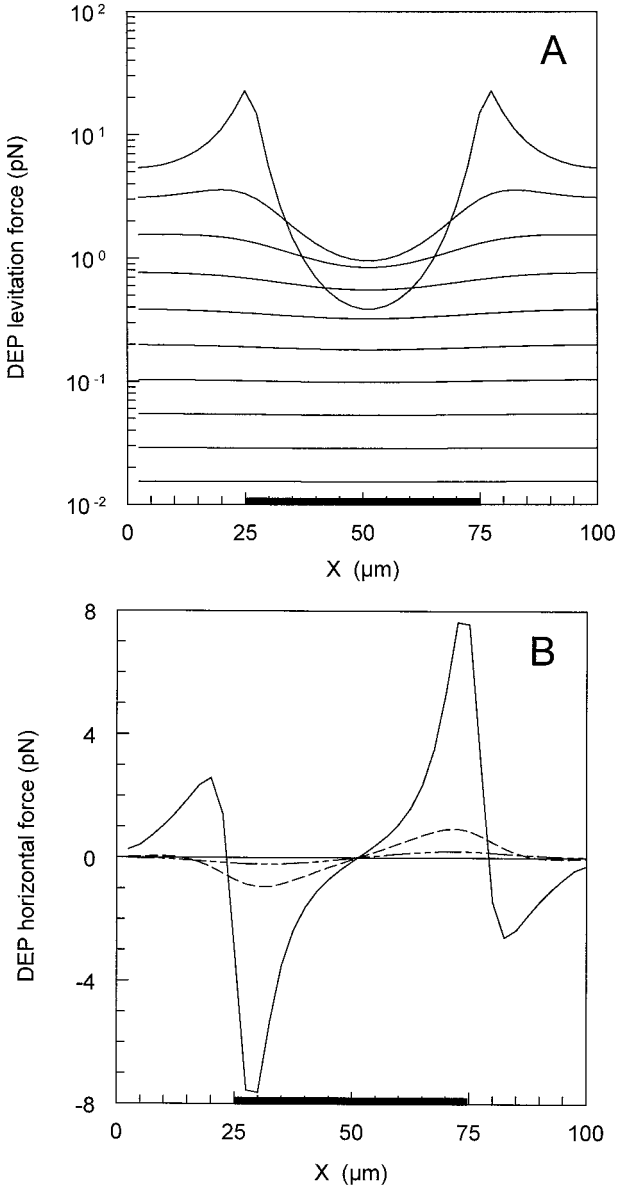

FIGURE 8 Dependencies of vertical (levitation, *A*) and horizontal (*B*) DEP forces on the particle position relative to electrode edges for a parallel electrode array of 50 μm width and spacing. The bold line on the x axis represents an electrode element. The electrical field simulation was performed using the Green's theorem-based analytical method (Wang et al., 1996). For the force calculation, a particle of radius $r = 5$ μm and $\mathrm{Re}(f_{CM}) = -0.5$ was subjected to an applied field of 1 V RMS. DEP levitation forces in (*A*) were calculated for particle heights between 5 (largest force) and 95 μm (smallest force) at 10 μm increments above the electrode plane. Levitation forces were found to be larger at positions over the electrode edges than over the central regions of the electrodes and gaps. The horizontal DEP forces shown in (*B*) were calculated for particle heights of 5 (—), 15 (- - -), and 25 (- · - · -) μm from the electrode plane. Positive and negative values correspond to the horizontal force component pointing with and against the direction of the x axis, respectively. Because of symmetry in electrode geometry and the resulting field distribution, the average horizontal DEP force is zero across one electrode/gap period.

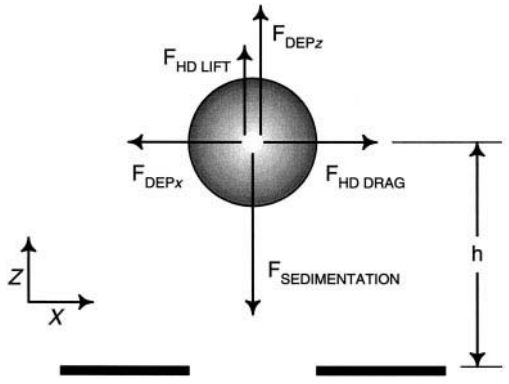

FIGURE 9 Schematic representation of the instantaneous forces acting on a particle in the DEP/G-FFF chamber.

(Fig. 8 *A*). As a particle travels across the electrode array, the *net* force it experiences in the vertical direction alternates around zero. As a result, the particle will move up and down, and the magnitude of these height perturbations will depend on the instantaneous DEP levitation forces, the fluid viscosity, and the rate of travel across the electrode elements. We found that the oscillation of particle heights was quite small (<2 μm) at moderate or high fluid flow rates (>200 μl/min) because particles had a short time (<20 ms) to respond to the variations in the vertical DEP force component. We therefore adopted a theoretical model in which it was assumed that particles are positioned at equilibrium heights in the flow profile that are determined by the balance of the *average* DEP levitation force with the constant sedimentation and HD lift forces (Huang et al., 1997). The oscillation of particle heights observed here is somewhat similar to the oscillation of particle velocities in a traveling-wave dielectrophoresis field reported by Hagedorn et al. (1992). Nevertheless, the oscillation magnitude here is much smaller than those in Hagedorn et al., because particles have little time to respond to the change in the DEP levitation force as they are carried quickly across the electrodes under the influence of the fluid flow.

In the fluid flow direction a particle experiences fluid drag as well as a horizontal component of DEP forces from the electrodes. Although the net fluid drag would be zero if a particle moved at constant velocity at a fixed height in the fluid flow profile in the absence of an applied electrical field, the horizontal DEP force component causes the particle velocity to suffer perturbations. Nevertheless, because of the electrode periodicity, the average horizontal DEP force over a complete electrode/gap period is zero (Fig. 8 *B*). Thus horizontal DEP forces have no effect on the average velocity of the particle. As a corollary, the velocity of particles depends only on their equilibrium height positions in the flow profile as determined by the balance of the average DEP levitation force and the sedimentation and HD lift forces; the horizontal DEP component does not influence particle velocities. This is one of the major differences between DEP/G-FFF and the early separation approach of DEP-retention. In that case, the horizontal DEP force component was used to compete with the fluid flow forces and thereby determine the particle elution rate (Becker et al., 1995; Markx et al., 1994; Talary et al., 1995).

Hydrodynamic lift forces

As discussed above, the balance of the average DEP levitation force and the sedimentation and HD lift forces determines particle equilibrium heights. To investigate the HD lift effect, G-FFF experiments were conducted where no DEP forces were applied so that particle equilibrium positions were determined solely by sedimentation and HD lift forces. The average velocities of PS beads of nominal diameter (6 and 15 μm) suspended in either deionized water or sucrose/dextrose buffers were measured as a function of the fluid flow rate (Fig. 10). Several trends were evident: 1) a near-linear dependency of the average velocity of PS beads on the fluid flow rate existed for each experimental condition; 2) for a given suspension condition and fluid flow rate, 15-μm PS beads traveled ~1.5 times faster than 6-μm beads; and 3) for a given flow rate, the velocities of PS beads were slightly higher in deionized water than in the sucrose/dextrose solution of higher viscosity and density.

Particle velocities under each flow condition (Fig. 10) were used to calculate the particle equilibrium heights due to the balance of HD lift and sedimentation forces. In the absence of particles, fluid flow in our chamber takes the form of a parabolic velocity profile. In general the velocity of a particle at a given height in such a flow profile is smaller than that of undisturbed fluid at the same height by a factor called the retardation coefficient. A number of

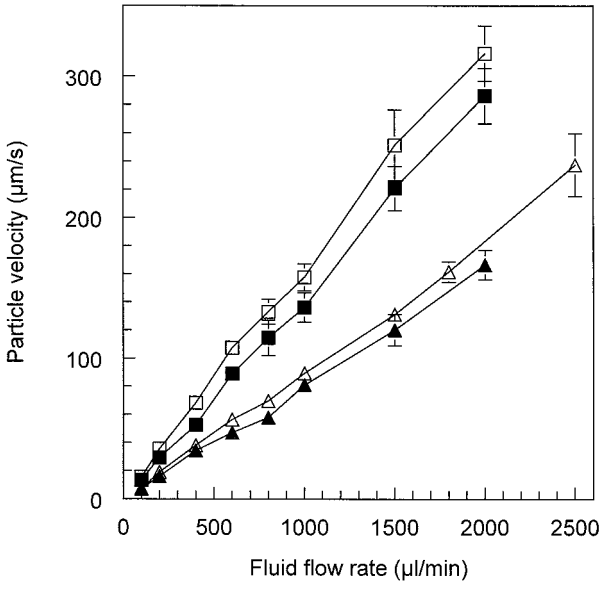

FIGURE 10 Dependency of the particle velocity on fluid flow rate for G/FFF operation. Results are shown for PS beads of 6 (△, ▲) and 15 μm (□, ■) are suspended in deionized water (△, □) and sucrose/dextrose solution (▲, ■). No electrical signals were applied to the electrode array.

authors have investigated this retardation effect under various flow conditions (Goldman et al., 1967; Press et al., 1986). Williams et al. (1992) summarized the findings, relating the particle velocity (V_p) to the velocity profile (V_m) through the retardation coefficient $f(h/r)$ in the expressions

$$V_p = f(h/r)V_m \tag{2}$$

where

$$f(h/r) = 1 - \frac{5}{16}\left(\frac{r}{h}\right)^3 \qquad \text{for } h > 1.1r$$

or

$$f(h/r) = \frac{0.74}{0.5 - 0.2\log[(h-r)/r]} \qquad \text{for } h < 1.1r.$$

and

$$V_m = 6\langle V_m\rangle \frac{h}{H}\left(1 - \frac{h}{H}\right) \tag{3}$$

given that h is the distance of the center of the particle to the chamber bottom surface and H is the chamber thickness. Using Eqs. 2 and 3, equilibrium positions (h) of the centers of PS beads in various G-FFF experiments were calculated as 7.92 ($\pm$0.13) and 8.1 ($\pm$0.13) μm for 15-μm, and 3.45 ($\pm$0.09) and 3.73 ($\pm$0.19) μm for 6-μm diameter beads in sucrose/dextrose solution and deionized water, respectively. Particle heights were essentially *independent* of the fluid flow rate. Thus, HD lift forces levitated PS beads only slightly and distances between particle peripheries and the chamber bottom wall were between only 0.4 and 0.7 μm. The lift force, equal to the sedimentation force for PS beads at the equilibrium positions, was dependent on particle size and suspending condition, but *not* on the fluid flow rate.

These results do not agree with a number of previous theoretical analyses of hydrodynamic effects where the lifting force was shown to be proportional to the first (Saffman, 1965; Williams et al., 1992) or second order (Ho and Leal, 1974) of the flow rate. The theories by Saffman (1965), Ho and Leal (1974), and Vassuer and Cox (1976) predict lifting forces two to three orders of magnitude smaller than those required to balance the sedimentation forces for PS beads at our observed particle equilibrium heights. On the other hand, the empirical formula for HD lift forces derived by Williams et al. (1992) predicts that PS beads should have been levitated to much higher positions than we observed. Furthermore, our findings that the HD lift force is independent of fluid flow rate and increases with decreasing fluid viscosity are contrary to the experimental results in several other reports (Caldwell et al., 1979; Parsons et al., 1996; Tong and Caldwell, 1995; Williams et al., 1992). The physical nature of the HD lift effect and the reasons for the discrepancies between our experimental data and these earlier findings are not understood. Clearly, further studies of the HD lift force are needed. Nevertheless, we note that PS beads typically moved at much higher velocities in DEP/G-FFF studies than in G-FFF experiments, demonstrating that DEP forces can levitate particles to much higher (up to 2 orders of magnitude) equilibrium positions than HD effects. We therefore conclude that hydrodynamic lift forces play little or no role in typical DEP/G-FFF separations.

Particle separation mechanics

Previously, we developed a theoretical model for DEP/G-FFF (Huang et al., 1997) in which the average DEP levitation force generated by parallel electrodes acting on a particle was given by

$$F_{DEPZ} = 2\pi A\, \varepsilon_m r^3\, \mathrm{Re}(f_{CM}) U^2 \exp(-4\pi h/d) p(f) \tag{4}$$

where U is the applied RMS voltage. Here, $\mathrm{Re}(f_{CM})$ is the real component of the Clausius-Mossotti factor, which reflects the magnitude and direction of field-induced polarization in the particle at frequency f (Sauer, 1985; Jones, 1995; Wang et al., 1995b; 1997). This factor is given by $f_{CM} = (\epsilon_p^* - \epsilon_m^*)/(\epsilon_p^* + 2\epsilon_m^*)$, where ϵ_p^* and ϵ_m^* are the frequency-dependent complex dielectric permittivities of the particle and its suspending medium. The parameter d is the periodicity of the parallel electrode array and A is a constant inversely proportional to d^3 ($= -176/d^3$) and relating to the exponential decay of the DEP levitation force as a function of height above the electrode plane (Fig. 11). For parallel electrodes of 50-μm widths and gaps, the parameter $d = 200$ μm and $A = -2.2072 \times 10^{13}$ m^{-3}. The function $p(f)$ is introduced to correct for the electrode polarization effect, which diminishes the electrical field that impinges on the particle (Schwan, 1992; Zhou et al., 1995; Huang et al., 1997). Ignoring the HD lifting effect, the particle equilibrium height h_{eq}, average particle velocity V_p, and particle retention time T can be derived as (Huang et al., 1997)

$$h_{eq} = \frac{d}{4\pi}\left\{2\ln(U) + \ln[Ap\,\mathrm{Re}(f_{CM})] + \ln\left(\frac{3\,\varepsilon_m}{2(\rho_p - \rho_m)g}\right)\right\} \tag{5}$$

and

$$V_p = \frac{3f(h_{eq}/d)\langle V_m\rangle d}{2\pi H}\left\{2\ln(U) + \ln[Ap\,\mathrm{Re}(f_{CM})] + \ln\left(\frac{3\varepsilon_m}{2(\rho_p - \rho_m)g}\right)\right\}\left\{1 - \frac{d}{4\pi H}\left[2\ln(U) + \ln[Ap\,\mathrm{Re}(f_{CM})] + \ln\left(\frac{3\varepsilon_m}{2(\rho_p - \rho_m)g}\right)\right]\right\} \tag{6}$$

$$T = L/V_p \tag{7}$$

where L is the chamber length. By using Eqs. 2–7, theoretical simulations of our experimental data were performed to allow us to derive the dielectric polarization factor $\mathrm{Re}(f_{CM})$ for PS beads under the various conditions noted earlier.

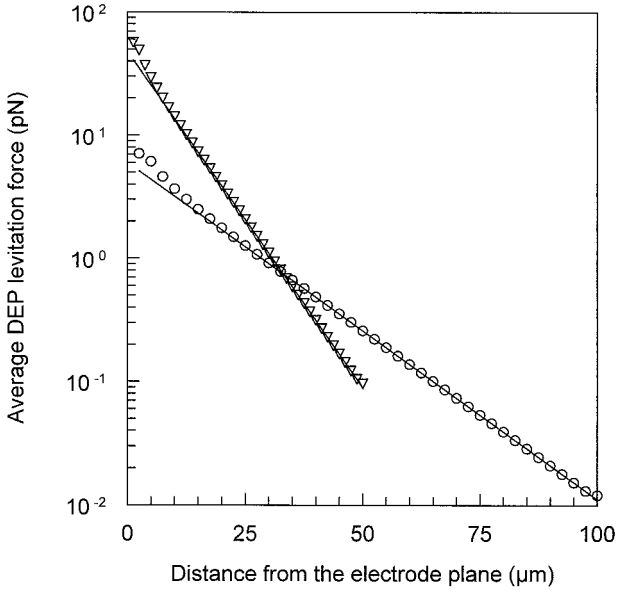

FIGURE 11 Dependency of the average DEP levitation forces on particle height above the parallel electrode plane for electrode widths (and gaps) of 50 (○) and 25 (▽) μm. The electrical field simulation was performed using the Green's theorem-based analytical method (Wang et al., 1996). For the force calculation, a particle of radius $r = 5$ μm and $\mathrm{Re}(f_{\mathrm{CM}}) = -0.5$ was subjected to an applied field of 1 V RMS. The solid lines are the best exponential curve fit (Eq. 4) to the average DEP forces calculated at each height. The DEP levitation force for the larger electrode width and gap (50 μm) decays slower than the smaller electrode geometry (25 μm). Note that the DEP force distributions for different-sized parallel electrode arrays are similar in form except for a factor in the force magnitude and a scaling in the geometrical coordinates.

Fig. 4 shows a comparison between the theoretical and experimental flow rate dependencies of retention times for 10 μm NF-PS and COOH-PS beads. Clearly, the theory is able to provide a good description of the experimental data, suggesting that our model is valid. Particle equilibrium heights were determined to be 65 μm for NF-PS beads and 71 μm for COOH-PS beads, almost two orders of magnitude larger than those attained by PS beads due to HD lift forces alone in G-FFF. These results again strongly suggest that DEP levitation forces are the dominant factor in controlling particle equilibrium positions in DEP/G-FFF; $\mathrm{Re}(f_{\mathrm{CM}})$ was derived as -0.20 and -0.28, for NF-PS and COOH-PS microbeads, respectively, at a frequency 50 kHz in sucrose/dextrose buffer of conductivity 10 mS/m. While it is not the purpose of this article to analyze the origin of the dielectric differences between NF-PS and COOH-PS beads, we note that a number of studies have been presented to characterize these particles (Arnold et al., 1987; Maier, 1997). Here we will briefly mention only some important points. COOH-PS beads are negatively charged because the carboxyl group is ionized to COO^- in our suspending medium of pH $\sim$7. NF-PS beads also possess some negative charges, a result of chemicals used in styrene polymerization during bead manufacture (Fischer and Nölken, 1988). These charges will induce counterion double layers around particles in suspension and the polarization of such double layers under the influence of an applied AC electric field contributes significantly to the dielectric properties of the particles (Grosse and Shilov, 1996; Maier, 1997). We consider that the difference observed here between the dielectric properties of NF-PS and COOH-PS beads is associated with differences in their electrical charges and the corresponding counterion double layers at the bead surfaces. Therefore, particle surface properties serve as the basis for DEP/G-FFF separation of NF-PS and COOH-PS beads.

The experimentally observed voltage dependency of particle elution times for NF-PS and COOH-PS beads was analyzed using Eqs. 2–7 using nonlinear fitting, and the results are shown in Fig. 5 *A*. Good agreement between theory and experiment is found for applied voltages $>$ 0.21 V RMS. Below 0.21 V RMS, the theory breaks down because the DEP force is predicted to be too small to levitate the particles. Theoretical particle elution times calculated by assuming a fixed particle levitation height due to the HD lifting forces alone in this low voltage regime were found to be larger than those observed experimentally. Furthermore, particles eluted faster with small voltages applied than with no DEP field. These data suggest that DEP forces *were* capable of levitating particles to some extent even for applied voltage below 0.21 V RMS. We believe that this discrepancy between our theoretical model and the experimental results for the low voltage regime arises from our assumption that DEP levitation forces can be averaged across an electrode width/gap period in order to calculate particle levitation characteristics. While the averaged DEP force may indeed not be sufficiently large to levitate particles, the much larger and highly localized DEP forces at positions over the electrode edges (Huang et al., 1997; Wang et al., 1996; Fig. 8 *A*) probably do levitate particles in those regions. Furthermore, our assumed exponential decay of average DEP forces with height above the electrode plane is a good approximation ($<$5% error) only at positions well above the electrode surface ($>$18 μm for parallel electrodes of 50-μm widths and spacing, Fig. 11) and does not hold for the small levitation heights in the low voltage regime. Another possible source of the discrepancy between the theoretical model and the experimental results in the low voltage regime is that the presence of particles was not taken into account in the field simulation (Fig. 8, *A* and *B*), resulting in less accurate determination of DEP forces.

Fig. 5 *B* shows that our theoretical model qualitatively fits the experimental voltage dependency observed for the elution time ratio between NF-PS beads and COOH-PS beads despite some discrepancies. As the applied voltage was reduced from 2.65 V to 0.21 V RMS, the elution time ratio increased and separation between the two PS microbead populations became greater. This higher discrimination at small operating voltages resulted from the fact that particles equilibrated at lower positions, where the fluid velocity gradient attained larger values. However, below 0.21 V RMS, HD lift forces contributed to the particle levitation, causing less differentiation in the equilibrium heights of

NF-PS and COOH-PS beads. This was because HD lift forces are not different for these particle types (NF-PS versus COOH-PS beads of similar size and density) as evidenced by the fact that NF-PS and COOH-PS beads could not be separated in G-FFF experiments. Separation of the two bead populations became impaired as the applied electrode voltage was decreased further.

Theoretical analyses were also made of the voltage dependencies of particle elution times for NF-PS beads of different size (Fig. 6). Values for $\mathrm{Re}(f_{CM})$ were derived as -0.12, -0.14, and -0.19 for NF-PS beads of 6, 10, and 15 μm diameter, respectively, at an applied field frequency of 50 kHz in sucrose/dextrose buffer having a conductivity of 2.2 mS/m. These differences in the dielectric properties were the basis for the DEP/G-FFF separation of PS beads of different sizes.

Optimization of DEP/G-FFF separation

It is evident from Eqs. 2–7 that the particle elution time is determined by a number of operational parameters, including the chamber height H and length L; the average fluid flow rate $\langle V_m \rangle$; the electrode periodic distance d; the applied voltage U; the particle radius r; the particle dielectric polarization parameter $\mathrm{Re}(f_{CM})$; and the particle and suspension densities ρ_p and ρ_m. Separation by DEP/G-FFF can therefore exploit differences in particle size, density, and dielectric properties. In the following we will discuss how the electrode and chamber dimensions, the applied field, and the particle suspension conditions influence the separation characteristics without invoking complex mathematical analysis based on differential calculus.

As in most FFF applications, it is assumed here that a parabolic flow profile exists in the vertical direction of the DEP/G-FFF chamber and that the shape of this profile is determined by the chamber height H. For achieving better separation performance, H should be chosen to maximize the fluid velocity gradient, given by

$$dV_m/dh = \frac{6\langle V_m \rangle}{H^2}(H - 2h) \tag{8}$$

The gradient dV_m/dh increases as the particle height is decreased in the flow profile so that better velocity differentiation is achieved for particles equilibrated closer to the chamber bottom surface. For particles having a maximum levitation height h_{max}, the choice of H will depend on the specific optimization criteria. For example, to maximize the average velocity gradient between 0 and h_{max}, the chamber height should be $2h_{max}$; to maximize the gradient at h_{max} the chamber height should be $4h_{max}$.

The particle elution time and the degree of separation between different particle types are proportional to the chamber length L (Eq. 7), thus better separation can be achieved by increasing L. The particle elution time is inversely proportional to $\langle V_m \rangle$ so that increasing the flow rate will result in faster separation. Nevertheless, at sufficiently high values of the fluid flow rate, the HD lift may impair particle separation. Other undesirable effects may also come into play at very high flow rates.

A large periodic distance d results in a slower exponential decay of DEP levitation forces with height above the electrode plane (Fig. 11), which in turn gives rise to a better discrimination in equilibrium heights of particles possessing subtle dielectric differences (Eqs. 5–7). Thus, electrode arrays with large d values are preferred for increasing the resolution of dielectric discrimination. Electrodes having large d values may, however, require a much higher field strength (E) to generate sufficiently strong DEP levitation forces (proportional to E^2/d). A higher field strength may in turn cause some undesirable effects, such as Joule heating of the suspending medium. Furthermore, as discussed earlier, the exponential decay relationship assumed for the average DEP levitation force above the electrode plane is accurate only for positions well above the electrode surfaces ($\sim$1/3 electrode width and gap, Fig. 11). Detailed analysis may be required for DEP force distributions close to the electrode surface to assess the effect of changing the periodic distance d for specific DEP/G-FFF applications. Such effects need to be considered when choosing the dimension parameter d of the electrodes.

As shown in Figs. 5 and 6, the applied voltage U is an important variable for DEP/G-FFF operation. Generally, large voltages levitate particles to higher equilibrium positions where the gradient of the fluid velocity is reduced. To exploit the region of large velocity gradient in the fluid flow profile for better particle separations, small voltages may be preferred. On the other hand, HD lift effects at low positions in the profile may complicate particle kinetic behaviors and small voltages also result in longer separation times. Clearly the applied voltages should be optimized for each application.

The density ρ_m of suspending medium is another important variable for DEP/G-FFF (Eqs. 5–7). For stable positioning of particles in the flow profile, negative dielectrophoretic forces and negatively buoyant particles should be used; ρ_m should therefore be smaller than the densities (ρ_p) of the particles (Gascoyne et al., 1996; Huang et al., 1997). The value for ρ_m is chosen based on the following criteria. If ρ_m is much smaller than ρ_p, then a large voltage and field strength may have to be applied to levitate the particles. On the other hand, if ρ_m is just slightly below ρ_p, then a long time is necessary for particles to relax to their equilibrium positions after introduction into the chamber (Eq. 1).

The applied field frequency f and the dielectric properties (electrical conductivity and permittivity) of suspending medium are important factors in determining the $\mathrm{Re}(f_{CM})$ of the particles (Gascoyne et al., 1997; Wang et al., 1997), and should be optimized by maximizing the differences in $\mathrm{Re}(f_{CM})$ between particles to be separated. As long as the applied DEP levitation forces (a function of the field frequency f and dielectric properties of suspending medium) are effective in controlling particle equilibrium heights in the flow profile, the DEP/G-FFF system can be used for

particle characterization and separation. In contrast to particle separations using DEP retention (Wang et al., 1993, Becker et al., 1995) where different particles must have different polarities for Re(f_{CM}), DEP/G-FFF separations require that different particles have different negative Re(f_{cm}) values. As shown previously in DEP/G-FFF (Huang et al., 1997), particle velocity (and therefore the retention time in Eq. 7) is very sensitive to Re(f_{CM}), suggesting considerably higher particle discriminations for DEP/G-FFF than for the DEP retention method.

CONCLUSIONS AND PERSPECTIVES

Dielectrophoretic/gravitational field-flow fractionation is an effective method for particle separation. It can be readily applied for the separation of particles of $\sim$1 μm to several hundred micrometers. It exploits not only differences in particle size and density, as in a number of other FFF techniques, but also, and most significantly, the particle dielectric properties. For biological cells, DEP/G-FFF separation can be based on differences in cell size, membrane capacitance and conductance (Gascoyne et al., 1997; Huang et al., 1997), and cell interior dielectric properties. For colloidal particles such as polystyrene beads, DEP/G-FFF separation can utilize differences in particle size, particle surface properties (such as surface charge), and bulk dielectric properties.

DEP levitation forces, generated by applying a relatively small AC voltage ($<$10 V p-p) to microelectrodes on the bottom surface of the separation chamber, are used to balance the gravitational (sedimentation) forces acting on the particles so as to position them in a flow velocity profile. Particles possessing different dielectric and density properties equilibrate at different heights and are carried at different velocities in a flow profile. As a result, different particles elute from the separation chamber at different times. The separation method is flexible because it depends on a number of operational parameters including the density and dielectric properties of the particle suspending medium and the voltage and frequency of the applied DEP field. These parameters may be varied to optimize separation performance for specific applications. The operational field frequency is typically above 1 kHz. This minimizes several undesired effects including electrode polarization and water electrolysis at electrode surfaces. The separation chamber can be readily miniaturized for applications demanding the use of even minute quantities of samples. Finally, DEP/G-FFF can be used to study the physical properties of particles. For example, the particle dielectric properties can be derived by determining the dependencies of their elution times on the frequency and voltage of the applied DEP field.

We thank Giovanni De Gasperis for help with particle counting using an imaging analysis system during our earlier DEP/G-FFF studies, and are grateful to Ying Huang, Xujing Wang, and Jun Yang for valuable discussions.

This work was supported in part by Electronics Technology Office of Defense Advanced Research Program Agency NRaD Contract N66001-97-C-8608 under DARPA Order E934, National Institutes of Health Grant R01 DK51065-01 from the National Institute of Diabetes and Digestive and Kidney Disease, and a Biomedical Engineering Research grant from the Whitaker Foundation.

REFERENCES

Andreux, J. P., A. Merino, M. Renard, F. Forestier, and J. P. Cardot. 1993. Separation of red blood cells by field flow fractionation. *Exp. Hematol.* 21:326–330.

Arnold, W. M., H. P. Schwan, and U. Zimmermann. 1987. Surface conductance and other properties of latex particles measured by electrorotation. *J. Phys. Chem.* 91:5093–5098.

Becker, F. F., X-B. Wang, Y. Huang, R. Pethig, J. Vykoukal, and P. R. C. Gascoyne. 1995. Separation of human breast cancer cells from blood by differential dielectric affinity. *Proc. Natl. Acad. Sci. USA.* 92:860–864.

Berg, H. C., and L. Turner. 1991. Selection of motile nonchemotactic mutants of *Escherichia coli* by field-flow fractionation. *Proc. Natl. Acad. Sci. USA.* 88:8145–8148.

Burt, J. P. H., R. Pethig, P. R. C. Gascoyne, and F. F. Becker. 1990. Dielectrophoretic characterization of Friend murine erythroleukemic cells as a measured of induced differentiation. *Biochim. Biophys. Acta.* 1034:93–101.

Caldwell, K. D., Z.-Q. Chang, P. Hradecky, and J. C. Giddings. 1984. Separation of human and animal cells by steric field-flow-fractionation. *Cell Biophys.* 6:233–251.

Caldwell, K. D., and Y.-S. Gao. 1993. Electrical field-flow fractionation in particle separation. I. Monodisperse Standards. *Anal. Chem.* 65: 1764–1772.

Caldwell, K., T. T. Nguyen, M. N. Meyers, and J. C. Giddings. 1979. Observation on anomalous retention in steric filed-flow-fractionation. *Sep. Sci. Technol.* 14:935–946.

Cardot, P. J. P., C. Elgea, M. Guernet, D. Godet, and J. P. Andreux. 1992. Size- and density-dependent elution of normal and pathological red blood cells by gravitational field-flow fractionation. *J. Chromatogr.* 654B:193–203.

Davis, J. M., and J. C. Giddings. 1986. Feasibility study of dielectric field-flow-fractionation. *Sepa. Sci. and Tech.* 21:969–989.

Fischer, J. P., and E. Nölken. 1988. Correlation between latex stability data determined by practical and colloid chemistry-based methods. *Prog. Colloid Polymer Sci.* 77:180–194.

Fuhr, G., W. M. Arnold, R. Hagedorn, T. Muller, W. Benecke, B. Wagner, and U. Zimmermann. 1992. Levitation, holding, and rotation of cells within traps made by high-frequency fields. *Biochim. Biophys. Acta.* 1108:215–223.

Fuhr, G., U. Zimmermann, and S. G. Shirley. 1996. Cell motion in time-varying fields: principles and potential. *In* Electromanipulation of Cells. U. Zimmermann and G. A. Neil, editors. CRC Press, Boca Raton. 260–328.

Gascoyne, P. R. C., Y. Huang, X.-J. Wang, J. Yang, G. DeGasperis, and X. B. Wang. 1996. Cell separation by conventional dielectrophoresis combined with field-flow-fractionation. *Biophys. J.* 70:330*a*.(Abstr.)

Gascoyne, P. R. C., Y. Huang, R. Pethig, J. Vykoukal, and F. F. Becker. 1992. Dielectrophoretic separation of mammalian cells studied by computerized image analysis. *Meas. Sci. Technol.* 3:439–445.

Gascoyne, P. R. C., J. Noshari, F. F. Becker, and R. Pethig. 1994. Use of dielectrophoretic collection spectra for characterizing differences between normal and cancerous cells. *IEEE Trans. Appl.* 30:829–834.

Gascoyne, P. R. C., X.-B. Wang, Y. Huang, and F. F. Becker. 1997. Dielectrophoretic separation of cancer cells from blood. *IEEE Trans. Appl.* 33:670–678.

Giddings, J. C. 1989. Field-flow fractionation of macromolecules. *J. Chromatogr.* 470:327–335.

Giddings, J. C. 1993. Field-flow fractionation: analysis of macromolecular, colloidal, and particulate materials. *Science.* 260:1456–1465.

Goldman, A. J., R. G. Rox, and H. Brenner. 1967. Slow viscous motion of a sphere parallel to a plane wall. II. Couette flow. *Chem. Eng. Sci.* 22:653–660.

Grosse, C., and V. N. Shilov. 1996. Theory of low-frequency electrorotation of polystyrene particles in electrolyte solution. *J. Phys. Chem.* 100:1771–1778.

Hagedorn, R., G. Fuhr, T. Müller, and J. Gimsa. 1992. Traveling-wave dielectrophoresis of microparticles. *Electrophoresis*. 13:49–54.

Ho, B. P., and L. G. Leal. 1974. Inertial migration of rigid spheres in two-dimensional unidirectional flows. *J. Fluid Mech.* 65:365–400.

Huang, Y., and R. Pethig. 1991. Electrode design for negative dielectrophoresis. *Meas. Sci. Technol.* 2:1142–1146.

Huang, Y., X. B. Wang, F. F. Becker, and P. R. C. Gascoyne. 1997. Introducing dielectrophoresis as a new force field for field-flow-fractionation. *Biophys. J.* 73:1118–1129.

Jones, T. B. 1995. Electromechanics of Particles. Cambridge University Press, Cambridge, UK. Chapt. 3, pp. 34–80.

Jones, T. B., and J. P. Kraybill. 1986. Active feedback-controlled dielectrophoretic levitation. *J. Appl. Phys.* 60:1247–1252.

Liu, L-K., P. S. Williams, M. N. Myers, and J. C. Giddings. 1991. Hydrodynamic relaxation in flow field-flow fractionation using both split and frit inlets. *Anal. Chem.* 63:2115–2122.

Maier, H. 1997. Electrorotation of colloidal particles and cells depends on surface charge. *Biophys. J.* 73:1617–1626.

Markx, G. H., Y. Huang, X. F. Zhou, and R. Pethig. 1994. Dielectrophoretic characterization and separation of microorganisms. *Microbiology.* 140:585–591.

Markx, G. H., J. Rousselet, and R. Pethig. 1997. DEP-FFF: field-flow-fractionation using nonuniform electric fields. *J. Liq. Chrom. & Rel. Technol.* 20:2857–2872.

Marszalek, P., J. J. Zielinski, and M. Fikus. 1989. Experimental verification of a theoretical treatment of the mechanism of dielectrophoresis. *Bioelectrochem. Bioenerg.* 22:289–298.

Parsons, R., V. Yue, X. Tong, P. J. P. Cardot, A. Bernard, J. P. Andreux, and K. Caldwell. 1996. Comparative study of human blood cell analysis with three different field-flow-fractionation systems. *J. Chromatog. B: Biomed. Appl.* 686:177–187.

Pethig, R. 1991. Application of A.C. electrical fields to the manipulation and characterisation of cells. *In* Automation in Biotechnology. I. Karube, editor. Elsevier, Amsterdam. 159–176.

Pethig, R., Y. Huang, X. B. Wang, and J. P. H. Burt. 1992. Positive and negative dielectrophoretic collection of colloidal particles using interdigitated castellated microelectrodes. *J. Phys. D: Appl. Phys.* 24: 881–888.

Pohl, H. A. 1978. Dielectrophoresis. Cambridge University Press, Cambridge (UK).

Pohl, H. A., and R. Pethig. 1977. Dielectric measurements using nonuniform electric field (dielectrophoretic) effects. *J. Phys. E.* 10:190–195.

Pohl, H., and K. Pollock. 1978. Electrode geometries for various dielectrophoretic force laws. *J. Electrostatics*. 5:337–342.

Press, W. H., B. P. Flannery, S. A. Teukolsky, and W. T. Vetlering. 1986. Numerical Recipes: The Art of Scientific Computing. Cambridge University Press, Cambridge, UK. 86–89.

Saffman, P. G. 1965. The lift on a small sphere in a slow shear flow. *J. Fluid Mech.* 22:385–400.

Sauer, F. A. 1985. Interaction forces between microscopic particles in an external electromagnetic field. *In* Interactions Between Electromagnetic Fields and Cells. A. Chiabrera, C. Nicolini, and H. P. Schwan, editors. Plenum Publishing Corporation, New York. 181–202.

Schwan, H. P. 1992. Linear and nonlinear electrode polarization and biological materials. *Ann. Biomed. Eng.* 20:269–288.

Talary, M., K. I. Mills, T. Hoy, A. K. Burnett, and R. Pethig. 1995. Dielectrophoretic separation and enrichment of CD34+ cell subpopulation from bone marrow and peripheral blood stem cells. *Med. Biol. Eng. Comp.* 33:235–237.

Tong, X., J. F. Ash, and K. D. Caldwell. 1997. Rapid swelling of a CHO-K1 aspartate/glutamate transport mutant in hypoosmotic medium. *J. Membr. Biol.* 156:131–139.

Tong, X., and K. D. Caldwell. 1995. Separation and characterization of red blood cells with different membrane deformability using steric field-flow-fractionation. *J. Chromatog. B.* 674:39–47.

Vasseur, P., and R. G. Cox. 1976. The lateral migration of a spherical particle in two-dimensional shear flows. *J. Fluid Mech.* 78:385–413.

Wang, X.-B., Y. Huang, F. F. Becker, and P. R. C. Gascoyne. 1995a. Dielectrophoretic manipulation of particles. *Conf. Record of IEEE, 30th IAS Meeting, Vol. 2.* 1358–1365.

Wang, X.-B., Y. Huang, J. P. H. Burt, G. H. Markx, and R. Pethig. 1993. Selective dielectrophoretic confinement of bioparticles in potential energy wells *J. Phys. D: Appl. Phys.* 26:1278–1285.

Wang, X.-B., Y. Huang, P. R. C. Gascoyne, and F. F. Becker. 1997. Dielectrophoretic manipulation of particles *IEEE Trans. Ind. Appl.* 33: 660–669.

Wang, X.-B., M. P. Hughes, Y. Huang, F. F. Becker, and P. R. C. Gascoyne. 1995b. Non-uniform spatial distributions of both the magnitude and phase of AC electric fields determine dielectrophoretic forces. *Biochim. Biophys. Acta*. 1234:185–194.

Wang, X., X.-B. Wang, F. F. Becker, and P. R. C. Gascoyne. 1996. A theoretical method of electrical field analysis for dielectrophoretic electrode arrays using Green's theorem. *J. Phys. D: Appl. Phys.* 29: 1649–1660.

Washizu, M., S. Suzuki, O. Kurosawa, T. Nishizaka, and T. Shinohara. 1994. Molecular dielectrophoresis of biopolymers. *IEEE Trans. Ind. Appl.* 30:835–843.

Williams, P. S., T. Koch, and J. C. Giddings. 1992. Characterization of near-wall hydrodynamic lift forces using sedimentation field-flow fractionation. *Chem. Eng. Comm.* 111:121–147.

Zhou, X.-F., G. H. Markx, R. Pethig, and I. E. Eastwood. 1995. Differentiation of viable and nonviable bacterial biofilm using electrorotation. *Biochim. Biophys. Acta*. 1245:85–93.